Spontaneous Symmetry Breaking in Single and Molecular Quantum Dots

Constantine Yannouleas and Uzi Landman
School of Physics, Georgia Institute of Technology, Atlanta, Georgia 30332-0430
(Received 30 December 1998)

Classes of spontaneous symmetry breaking at zero and low magnetic fields in single quantum dots (QD's) and quantum dot molecules (QDM's) are discussed in relation to the ratio R_W between the interelectron Coulomb repulsion and the harmonic confinement, using spin-and-space unrestricted Hartree-Fock calculations. These include Wigner crystallization for $R_W > 1$, and formation of noncrystallized electron puddles localized on the individual dots in QDM's, as well as spin-density waves in single QD's, for $R_W < 1$. [S0031-9007(99)09495-8]

PACS numbers: 73.20.Dx, 71.45.Lr, 73.23.–b

Two-dimensional (2D) electron gases, have provided (e.g., the fractional quantum Hall effect [1,2]), and continue to provide (e.g., a charge-density wave at higher Landau levels [3]), a source of discovery of remarkable many-body phenomena. Recently, 2D artificial quantum dots (QD's) and quantum dot molecules (QDM's) have become available, with the capability of controlling the dots' size, shape, and number N of electrons [4,5].

Single QD's are commonly referred to as "artificial atoms," since interpretations of transport and capacitance experiments draw often on analogies between such artificial structures and natural atoms [4,5]. Underlying these analogies is an effective (circular) central mean field (CMF) picture, with the electronic spectra exhibiting (at zero magnetic field) shell closures and following Hund's rules for open shells. Indeed, in experiments on single QD's, the addition energy (AE) spectra [4] exhibit maxima at the expected closed shells ($N = 2$, 6, and 12), and at the midshells ($N = 4$, 9, and 16) in accordance with Hund's rule.

Here, using the self-consistent spin-and-space unrestricted Hartree-Fock (sS-UHF) [6,7] method, we discuss, for zero and low magnetic fields (B), three types of spontaneous symmetry breakings (SB) in circular single QD's and in lateral QDM's (i.e., formation of ground states of lower symmetry than that of the confining potentials [12]). These include the following: (I) Wigner crystallization (WC) [13] in both QD's and QDM's, i.e., (spatial) localization of individual electrons, (II) formation of electron puddles (EP's) in QDM's, that is, localization of the electrons on each of the individual dots comprising the QDM, but without crystallization within each dot, and (III) pure spin-density waves (SDW's) which are not accompanied by spatial localization of the electrons [9]. Furthermore, we show that CMF descriptions at zero and low magnetic fields may apply only for low values of the parameter $R_W \equiv Q/\hbar\omega_0$, where Q is the Coulomb interaction strength and $\hbar\omega_0$ is the parabolic confinement; $Q = e^2/\kappa l_0$, with κ being the dielectric constant, $l_0 = (\hbar/m^*\omega_0)^{1/2}$ the spatial extension of the lowest state's wave function in the parabolic confinement, and m^* the effective electron mass. With the sS-UHF, we find that WC occurs (SB of type I) in both QD's and QDM's for $R_W > 1$. For QDM's with $R_W < 1$, WC does not develop and instead EP's may form (SB of type II). We note here that while certain quantum-mechanical studies of electron localization (WC at high B) in single QD's have been discussed previously [8,14], this is the first study to explore, using a self-consistent quantum-mechanical treatment, broken symmetry WC and EP states in the $B = 0$ and small B regimes for both circular single QD's and lateral QDM's, thus providing new insights into the nature of these systems. Additionally, for single QD's with $R_W < 1$ and $N \leq 20$, we find that in the majority of cases the ground states exhibit CMF behavior without symmetry breaking; however, in several instances (e.g., $N = 14$), a pure SDW (SB of type III) develops.

The many-body Hamiltonian for our problem is $\mathcal{H} = \sum_{i=1}^{N} H(i) + \sum_{i<j}^{N} e^2/\kappa|\mathbf{r}_i - \mathbf{r}_j|$, where the second term corresponds to the interelectron Coulomb repulsion. The single-particle Hamiltonian $H(i) = H_0(i) + V_{\rm neck}(i) + H_B(i)$ contains a term describing the motion of an electron in a 2D two-center-oscillator (TCO) [15] confinement, i.e., $H_0(i) = \mathbf{p}_i^2/2m^* + m^*\omega_0^2(x_i^2 + y_{t,i}'^2)/2$, where $y_{t,i}' = y_i - \tilde{y}_t$; $t = l$ for $y_i < 0$ (left) and $t = r$ for $y_i > 0$ (right), with $\tilde{y}_l < 0$ and $\tilde{y}_r > 0$ being the centers of the left and right oscillators. In the QDM, the dots are joined smoothly via a neck described by the term $V_{\rm neck}(i)$ (4th-order polynomial in $y_{t,i}'$ [11,15]) which allows variations of the bare interdot barrier height (V_b) for any distance $d = \tilde{y}_r - \tilde{y}_l$; for $d = 0$, the system reduces to a single harmonically confined QD. Magnetic-field effects are included in $H_B(i) = [(\mathbf{p}_i - e\mathbf{A}/c)^2 - \mathbf{p}_i^2]/2m^* + g^*\mu_B\mathbf{B}\cdot\mathbf{S}_i/\hbar$, where $\mathbf{A}_i = B(-y_i/2, x_i/2, 0)$ and the last term is the Zeeman interaction with an effective factor g^*, $\mathbf{S}_i$ is the electron spin, and μ_B is the Bohr magneton. To solve the sS-UHF equations [16], we use a (variable with d) basis consisting of the eigenstates of $H_0(i)$ [due to its separability, the eigenfunctions of $H_0(i)$ can be expressed as products of 1D harmonic-oscillator wave functions in x_i and parabolic cylinder functions in

$y'_{t,i}$ [15]]. In all calculations, we used $m^* = 0.067m_e$ (GaAs) and $\hbar\omega_0 = 5$ meV. For κ, we used the GaAs value of 12.9 (i.e., $R_W = 1.48$), as well as $\kappa = 20$ (i.e., $R_W = 0.95$, corresponding to a weakened interelectronic repulsion, due, e.g., to the effect of the finite thickness of the dots).

The spatial distributions of the electronic densities for QD's and QDM's reveal in almost all cases that for $R_W = 1.48$ (i.e., $\kappa = 12.9$) the ground-state solutions are Wigner crystallized. An example of such a (finite) Wigner crystal with $B = 0$ is shown in Fig. 1(a) for a $d = 70$ nm $(-\tilde{y}_l = \tilde{y}_r = 35$ nm), $V_b = 10$ meV closed-shell QDM with $N = 12$. The WC is portrayed by 6 well-resolved humps (3 in each well) for both the up (↑) and down (↓) spins, and by 6 humps and 6 troughs for the spin density (↑ − ↓); note that the density peaks for the two spin directions do not overlap. Formation of such "Wigner supermolecules" (WSM's) in QDM's is analogous to that of "Wigner molecules" (WM's) [14] in single QD's. The appearance of such a WC is a consequence of the large value of R_W (1.48 in this case).

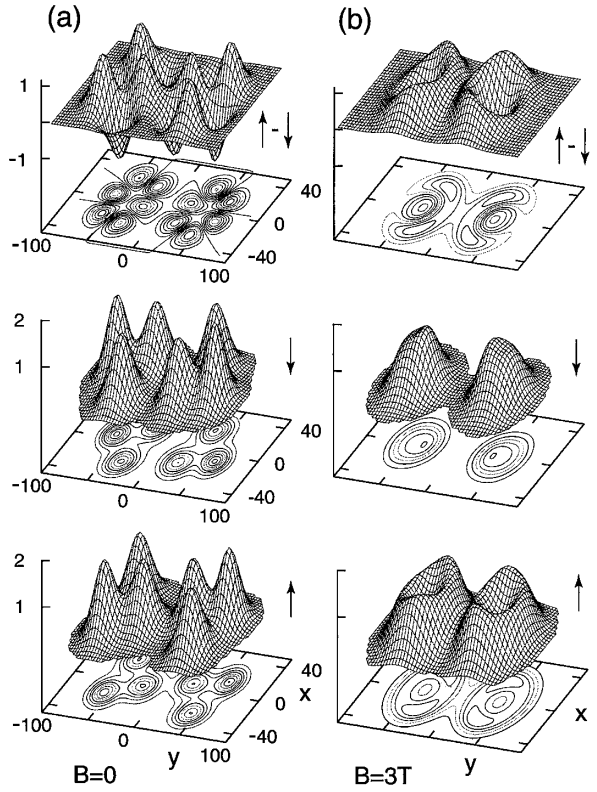

FIG. 1. sS-UHF results for a $12e$ QDM ($d = 70$ nm, $V_b = 10$ meV, $\hbar\omega_0 = 5$ meV), without [in (a)] and with a magnetic field $B = 3$ T [in (b)]. For both cases, the bottom and middle panels correspond to the up-spin and down-spin electron distributions, respectively, and the top ones correspond to the difference between them (spin density). Lengths (x and y axes) in nm, density distributions (vertical axes) in 10^{-3} nm^{-2}. The x-axes, y-axes, and vertical-axes scales in (b) are the same as in (a).

The mean distance between neighboring density maxima inside each of the coupled dots equals $\bar{r} \approx 20$ nm, i.e., roughly twice larger than the effective Bohr radius $a_B^*(\kappa = 12.9) = \hbar^2\kappa/m^*e^2 = 10.188$ nm. Inspection of the wave functions shows that this case corresponds to an intermediate electron-density regime, where spatial localization of *individual* electrons emerges, but with finite-amplitude contributions of each of the wave functions to several of the density peaks (i.e., "weak" WM, see below); full localization into a "classical" WC requires even lower densities [17].

A magnetic field compresses the electronic orbitals in the QDM and the consequent increase in Coulomb repulsion promotes electrons to higher orbitals of larger spatial extension, with an increase in the spin polarization (spin flip) resulting in optimization of exchange-energy gain (for a description of such a process in single QD's, see Ref. [5]). An example is shown for the QDM in Fig. 1(b) for $B = 3$ T ($g^* = -0.44$), where two of the down-spin electrons flipped, resulting in 8 up-spin and 4 down-spin electrons, accompanied by a reduced Wigner crystallinity (partial "melting") of the WSM, portrayed by the less pronounced density peaks [compare Fig. 1(b) with Fig. 1(a)], and increased density in the interdot region.

Having discussed formation of a WSM (in a $12e$ closed-shell QDM) made of Wigner molecules in each of the coupled dots, we display in Fig. 2 results, with $B = 0$, for the ground state (singlet) of a closed-shell ($N = 6$) single QD for two values of κ. For $\kappa = 12.9$ (i.e., $R_W = 1.48$), we observe again the emergence of a WM; note in Fig. 2(a), bottom, the six charge-density maxima arranged on a ring, with $\bar{r} \approx 20$ nm. On the other hand, for the same single QD, but with a reduced Coulomb repulsion ($\kappa = 20$, $R_W = 0.95$), no WC occurs; compare the charge densities in Figs. 2(b) and 2(a). Thus by varying R_W, one may cross the "phase boundary" separating the localized Wigner-crystallization and delocalized (CMF) regimes. Furthermore, in the WC regime the electron (charge) localization is accompanied here by a SDW [see top panel in Fig. 2(a) and also in Fig. 1(a)].

The WM emerging for $R_W = 1.48$ [Fig. 2(a)] is a weak one. The transition into the "strong"-WM regime, caused by an increase in the strength of the Coulomb repulsion, is illustrated in Fig. 2(c) for the same QD but with $\kappa = 6$, i.e., $R_W = 3.18$. The two WM isomers shown exhibit sharper electron density peaks reflecting stronger localization (seen also from much reduced wave-function amplitudes at neighboring sites). The geometries of the lower-energy fully spin-polarized, $P \equiv N\uparrow - N\downarrow = 6$, isomer [Fig. 2(c), right], and that of the higher-energy isomer with $P = 0$ [Fig. 2(c), left] agree well with those determined classically (i.e., for $R_W \to \infty$) [18].

Consider next an open-shell ($N = 6$) QDM with $d = 70$ nm, $V_b = 10$ meV, and $R_W = 1.48$, for which CMF-type treatments [as well as local spin density (LSD) functional [11]] predict a total net spin polarization $P = 2$ in

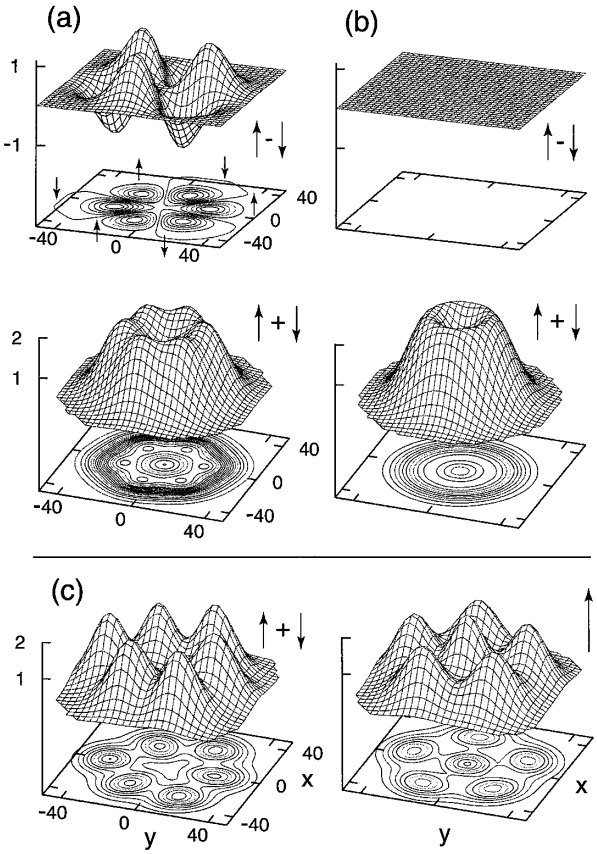

FIG. 2. Total electronic density distributions [bottom of (a) and (b); and panel (c)], and spin density distributions [top of (a) and (b)] for a $6e$ single QD with $\hbar\omega_0 = 5$ meV and $B = 0$; $\kappa = 12.9$ ($R_W = 1.48$) in (a), $\kappa = 20$ ($R_W = 0.95$) in (b), and $\kappa = 6.0$ ($R_W = 3.18$) in (c). The spin polarizations are $P = 0$ in (a), (b), and [(c), left], and $P = 6$ for the isomer in [(c), right] whose energy is lower by 1.72 meV than that of the one shown in [(c), left]. Units as in Fig. 1.

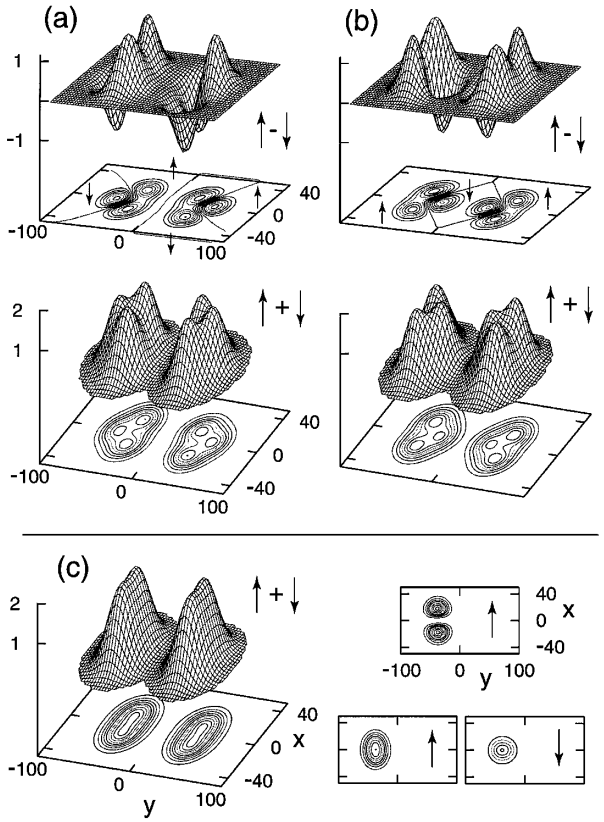

FIG. 3. (a) Ground-state and (b) an excited-state Wigner-crystallized total electronic (charge) density distributions (bottom panels) and spin-density distributions (top) for a $6e$ QDM with $\hbar\omega_0 = 5$ meV, $d = 70$ nm, $V_b = 10$ meV, $\kappa = 12.9$, and $B = 0$. (c), left: Total electronic density for the same QDM, but with $\kappa = 20$, illustrating formation of (noncrystallized within the dots) EP's. (c), right: Contour plots of the densities of the three individual orbitals localized on the left dot ($P_l = 1$, with spin polarization of the orbitals as indicated). Units as in Fig. 1.

accordance with Hund's rule, while we find here that the ground state of the QDM is a Wigner-crystallized singlet, i.e., $P = 0$ [see Fig. 3(a)], consisting of two spin-polarized (triplet) WM's [formed inside the left and right dots; see Fig. 3(a), top]. An excited state of the molecule (with a 0.09 meV higher energy) shown in Fig. 3(b) is also crystallized but with a net spin polarization $P = 2$; note the different spatial configurations of the ground and excited states. Reducing the R_W value for the QDM to 0.95 (i.e., $\kappa = 20$) transforms the ground state of the $6e$ QDM from the crystallized state [Fig. 3(a)] into one consisting of electron puddles [SB of type II, Fig. 3(c), left]; here each of the EP's (on the left and right dots) is spin polarized with $P_l = 1$, $P_r = -1$, and the singlet and triplet states of the whole QDM are essentially degenerate. Note that the orbitals on the left and right dots [see, e.g., those on the left dot in Fig. 3(c), right] are those expected from a CMF treatment, but with slight (elliptical) distortions due to the interdot interaction. Only for much lower values of R_W ($\lesssim 0.20$, i.e., $\kappa \gtrsim 90.0$) Fermi liquid (delocalized) behavior is restored.

Results of sS-UHF calculations at $B = 0$ for the AE's, $\Delta\varepsilon = E(N+1) - E(N) - [E(N) - E(N-1)]$, where $E(N)$ is the N-electron total energy, are shown for single QD's and QDM's in Fig. 4. For the single QD's and for a rather wide range of $R_W > 1$ (e.g., see the curve marked $\kappa = 12.9$), the AE's (corresponding mostly to WC states) exhibit maxima at the same values of N (see introductory paragraphs) as in the "normal" (i.e., $R_W < 1$ noncrystallized, CMF) regime. However, while in the latter the spin polarizations follow Hund's rule (except for $N = 14$, corresponding to a pure SDW state), those in the WC states ($\kappa = 12.9$) for $N \geq 8$ do not. For the QDM, a CMF treatment predicts for sufficiently large interdot barriers (e.g., $V_b = 10$ meV) shell closures at $N = 4$ and 12 (i.e., twice the single QD values) and (Hund's) half-shell maximum spin polarizations (e.g., at $N = 8$). While shell-closure features are observed in the

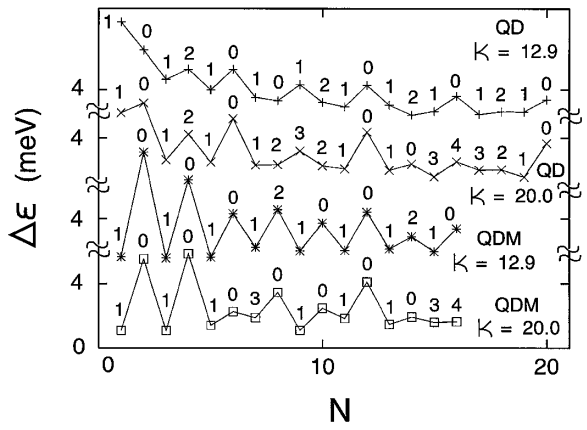

FIG. 4. sS-UHF results for the addition energies ($\Delta\varepsilon$ vs N) of a single QD ($\hbar\omega_0 = 5$ meV, two upper curves) and for a QDM ($\hbar\omega_0 = 5$ meV, $d = 70$ nm, $V_b = 10$ meV) calculated for $\kappa = 12.9$ and 20, and for $B = 0$. Energies in meV. The spin polarizations, $P = N\uparrow - N\downarrow$, are marked on the curves.

AE's of the QDM's with $\kappa = 12.9$ (WC) and $\kappa = 20$ [where EP's may form, see, e.g., Fig. 3(c)] shown in Fig. 4 (more pronounced for $\kappa = 20$), in both cases the spin polarizations do not in general follow Hund's rule (e.g., $N = 6$ and 8).

In summary, using sS-UHF calculations, we discussed three classes of spontaneous SB in QD's and QDM's at zero and low magnetic fields, i.e., formation of Wigner crystallized molecules and supermolecules for $R_W > 1$, and noncrystallized electron puddles localized on the individual dots in QDM's, as well as pure SDW's in single QD's (for $R_W < 1$). Further studies of such broken symmetries may include mapping of "phase boundaries" through variations of materials dependent (e.g., dielectric constant) and externally controlled (e.g., gate voltages, interdot distances and barrier heights, and magnetic fields) parameters, and probing of excitations and spin polarizations [19].

This research is supported by the U.S. D.O.E. (Grant No. FG05-86ER-45234).

[1] D. C. Tsui, H. L. Störmer, and A. C. Gossard, Phys. Rev. Lett. **48**, 1559 (1982).
[2] R. B. Laughlin, Phys. Rev. Lett. **50**, 1395 (1983).
[3] M. P. Lilly *et al.*, Phys. Rev. Lett. **82**, 394 (1999).
[4] S. Tarucha *et al.*, Phys. Rev. Lett. **77**, 3613 (1996).
[5] R. C. Ashoori, Nature (London) **379**, 413 (1996).
[6] Y. G. Smeyers, in *Self-Consistent Field: Theory and Applications*, edited by R. Carbó and M. Klobukowski (Elsevier, New York, 1990), p. 80.
[7] Our sS-UHF employs N (mean-field) effective potentials and differs from the usual (restricted) HF in two ways: (i) It employs different orbitals for different spin directions and (ii) it relaxes the requirement that the electron wave functions be constrained by the symmetry of the external confining field. Earlier HF studies of single QD's did not incorporate the spin-and-space unrestrictions simultaneously. For example, Wigner molecules (at $B = 0$ and/or finite B) were not found by D. Pfannkuche *et al.* [Phys. Rev. B **47**, 2244 (1993)] and M. Fujito *et al.* [Phys. Rev. B **53**, 9952 (1996)]. Indeed, using symmetry-restricted variational wave functions, we have reproduced the results of these studies, while with the sS-UHF, with no such restrictions, broken-symmetry solutions with lower energy were obtained as described here. We further note here that employing a space-UHF, but only for fully polarized single QD's (i.e., under high magnetic fields where the spin unrestriction is not at play), Wigner crystallization has been investigated [8]. LSD calculations [9–11] where there are only two effective potentials (associated with the two spin directions) cannot yield in general crystallized solutions (except for $N = 2$ in a deformed single QD and in a QDM [11]). While certain symmetry breaking can be obtained with LSD (e.g., pure SDW [9]), spatial localization may require self-interaction corrections (SIC-LSD) [J. P. Perdew and A. Zunger, Phys. Rev. B **23**, 5048 (1981); R. O. Jones and O. Gunnarsson, Rev. Mod. Phys. **61**, 689 (1989)].
[8] H.-M. Müller and S. E. Koonin, Phys. Rev. B **54**, 14 532 (1996).
[9] M. Koskinen *et al.*, Phys. Rev. Lett. **79**, 1389 (1997).
[10] I-H. Lee *et al.*, Phys. Rev. B **57**, 9035 (1998).
[11] R. N. Barnett *et al.*, Eur. Phys. J. D (to be published).
[12] (a) J. Paldus, in *Self-Consistent Field: Theory and Applications* (Ref. [6]), p. 1. For a general discussion of SB and the associated emergence of highly degenerate manifolds of excitations (Goldstone modes) see the following: (b) P. W. Anderson, *Basic Notions of Condensed Matter Physics* (Benjamin, Menlo Park, CA, 1984) and (c) P. Ring and P. Schuck, *The Nuclear Many-Body Problem* (Springer, New York, 1980), in the context of SB in finite systems and restoration of broken symmetries (Chap. 11); (d) D. J. Thouless, Nucl. Phys. **21**, 225 (1960).
[13] E. Wigner, Phys. Rev. **46**, 1002 (1934).
[14] P. A. Maksym, Physica (Amsterdam) **184B**, 385 (1993).
[15] For 3D TCO's for nuclei and clusters, see J. Maruhn and W. Greiner, Z. Phys. **251**, 431 (1972); C. Yannouleas and U. Landman, J. Phys. Chem. **99**, 14 577 (1995).
[16] The sS-UHF equations were solved using the Pople-Nesbet-Roothaan formalism [A. Szabo and N. S. Ostlund, *Modern Quantum Chemistry* (McGraw-Hill, New York, 1982), p. 214].
[17] For a study of 1D single QD's, see K. Jauregui *et al.*, Europhys. Lett. **24**, 581 (1993).
[18] F. Bolton and U. Rössler, Superlattices Microstruct. **13**, 139 (1993).
[19] This includes spectroscopical probing of the intrinsic electronic spectra of the SB states, and of the rotational and vibrational spectra (Goldstone modes [12(b) and (c)]) of the symmetry broken states (WM's and EP's) using radio and/or microwave frequencies (and possibly employing polarized radiation), as well as studies of the effect of impurities on the formation of SB states and their spectra; for investigations of impurity-pinning effects, see Ref. [11] and C. Yannouleas and U. Landman (to be published).